A Systematic and Topologically Stable Conformal Finite-Difference Time-Domain Algorithm for Modeling Curved Dielectric Interfaces in Three Dimensions

Theodoros I. Kosmanis, *Student Member, IEEE,* and Theodoros D. Tsiboukis, *Senior Member, IEEE*

***Abstract*—A systematic conformal finite-difference time-domain (FDTD) algorithm for the direct modeling of dielectric interfaces in three dimensions is presented in this paper. The straightforward procedure is based on the proper reformation of the grid cells in the vicinity of the dielectric surface, leading thus to the creation of five-faced prisms on the primary grid, apart from the standard hexagonal ones. The new scheme overcomes any topological deficiency that forbids the contour path FDTD and conformal FDTD technique to directly simulate dielectric boundaries, since it maintains the lattice duality. Therefore, no instabilities, even late-time ones, are observed. On the other hand, the accuracy obtained, even with very coarse meshes, is very good as is proved by the numerical analysis of various resonance problems.**

***Index Terms*—Conformal finite-difference time-domain (CFDTD), dielectric interfaces, resonators.**

I. Introduction

SINCE the advent of the finite-difference time-domain (FDTD) method, many efforts have been made in order to produce an efficient and straightforward algorithm for the geometric modeling of arbitrarily shaped surfaces [1]. The quite popular staircase meshing, though it fulfills the simplicity condition, is known to introduce significant errors, especially in resonance problems, even if very dense meshes are incorporated [2], [3]. On the other hand, the appreciable number of FDTD variations, promising to obtain sufficient simulation of non-Cartesian structures, is fairly complex or characterized by limited applicability.

Specifically, for purely cylindrical or spherical problems, the FDTD method in global curvilinear coordinates (cylindrical or spherical) [1] or special two-dimensional (2-D) reductions due to rotational symmetry (body of revolution) [4], [5] are successfully utilized. However, both cases are limited by the fact that the curvilinear grid must conform to all the boundaries and interfaces of a problem, otherwise another mesh must be selected.

These restrictions are overcome by the generally nonorthogonal FDTD methods [6]–[9], which are no longer based on orthogonal grids but on arbitrarily structured ones that geometrically model the problem's boundaries. Their significant efficiency is outbalanced by the great deal of computational resources and programming complexity required, since, in addition to the original FDTD algorithm, lattice information must also be stored.

The research for a more simple (than the nonorthogonal FDTD), with wider applications (than the global curvilinear FDTD) and more accurate (than staircase meshing) algorithm led to the contour path finite-difference time-domain (CPFDTD) technique [10], [11], the conformal finite-difference time-domain (CFDTD) technique [12], and their numerous variations [13]–[17]. They are all based on a reformulation of the original FDTD method in terms of surface and contour integrals.

The objective of this paper is to present a new consideration of the contour path and conformal FDTD approaches by means of the grid structure. A systematic procedure, which maintains the reciprocity and causality of Maxwell's equations (absent in the original CPFDTD algorithm) and is directly applicable to dielectric boundaries in three dimensions, is built. The grid cells are distorted from their Cartesian form only near the dielectric interface according to the FDTD conformal techniques, while right afterwards appropriate edge movements are performed. In the lattice created, new types of cells, apart from the classical orthogonal and conformal ones, appear (five-faced primary prisms and seven- and nine-faced dual prisms). Therefore, a topologically correct scheme is generated where the two grids, accommodating the electric and magnetic field components, maintain their duality. The field variables are updated by means of the integral form of Maxwell's equations, which are now feasibly implemented. The proposed procedure is thoroughly analyzed in Section III, after a brief description of the CPFDTD and CFDTD approaches in Section II. Finally, the efficiency of the innovative algorithm is demonstrated through the solution of various demanding resonance problems.

II. Modeling of Curved Surfaces With the FDTD Method

A. CPFDTD Technique

The method is a generalization of the original FDTD algorithm. It is based on the local deformation of the lattice cells

Manuscript received January 30, 2002; revised September 16, 2002.

The authors are with the Department of Electrical and Computer Engineering, Aristotle University of Thessaloniki, Thessaloniki, GR-54126 Greece (e-mail: tsibukis@eng.auth.gr).

Digital Object Identifier 10.1109/TMTT.2003.808617

in the vicinity of the curved surface in order to geometrically conform to it, whereas in the rest of the computational domain the grid preserves its initial orthogonality [10], [11]. Therefore, the necessary boundary or interface conditions on the surface—for example, the continuity of the tangential electric field along a dielectric interface—can be easily implemented. Due to this locally nonorthogonal grid structure, the update equations are not derived from the differential form of Maxwell's equations (standard FDTD) but from the integral one, which are discretized so as to maintain the leapfrog character in space and time.

Consequently, considering a 2-D grid with E_x, E_y, and H_z components as variables, the Faraday contours, used for the update of the H_z components, are deformed near the conducting or dielectric surface, enforcing an edge to align with it. On the other hand, the magnetic field components remain at the center of the initial cells and, hence, Ampere's contours, used for the update of the electric field, remain orthogonal. It must be noted that calculations of Ampere's contours crossing the interface are either not performed (conducting objects) or performed by means of interpolation procedures or the nearest neighbor approximation (conducting/dielectric objects) [10].

In any case, these are sources of inaccuracy and inherent instability (independent of the time step selection), since they are responsible for the noncausality and the nonreciprocity of the algorithm [16], [18]. Thus, although simple and efficient, the CPFDTD method frequently leads to instabilities.

Efforts have been made toward a stable procedure; however, these improvements are valid only for the simulation of conducting materials and not for dielectric objects [13], [15], [19].

B. CFDTD Technique

This method, a representative version of which has been presented for the modeling of perfectly conducting objects [12], varies from the CPFDTD algorithm in the treatment of the magnetic field. In an effort to overcome the instability problems that reside in the CPFDTD, magnetic field components, located at the center of distorted cells but inside the perfectly conducting material are also computed. This is obtained by taking into account the nonzero components of the electric field in the cell surrounding the corresponding magnetic field component and the edge lengths outside the conductor. Therefore, each electric field component can be calculated by means of Ampere's law and not by any other auxiliary way. However, the method has some stability limitations, which are outbalanced by using the CPFDTD complementarily to the CFDTD [12]. Nevertheless, it is considered to be more efficient as compared to the CPFDTD when modeling conducting materials [16].

C. Modeling Dielectric Objects in Three Dimensions: The "Stair-Step" Problem

The two aforementioned techniques are proved to be inefficient for the direct simulation of dielectric interfaces in three dimensions [16], mainly because the tangential to the boundary electric field component of the distorted cells is no longer zero.

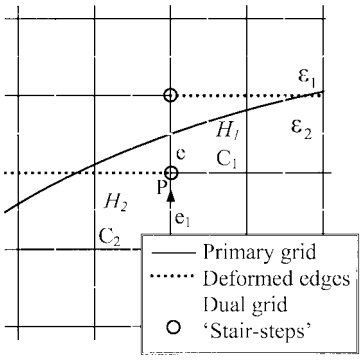

Fig. 1. The "stair-step" appears because P is the node of cell C_1, but not of the neighboring one, C_2.

Consequently, the so-called "stair-step" problem appears and renders the locally nonorthogonal structure topologically unstable.

To probe further, let us assume a dielectric interface that is arbitrary in shape, according to a function $y = f(x)$ with x and y corresponding to the two dimensions of the structure's cross section, while no alteration occurs in the third one (z). Fig. 1 illustrates its discretization by an orthogonal finite difference grid, which would actually be the lattice used by the CPFDTD and the CFDTD.

Inspecting a wider part of the computational space (not only the restricted area of two cells), one can easily observe the "stair-step" problem, which arises in the primary grid when the pair of distorted cells moves a row up or down according to the curve's slope. As shown in Fig. 1 (z cross section), the "stair-step" is created by a cell (C_1) node (P) that does not coincide with a corresponding node of a neighboring cell (C_2), but is located along their common edge (e). This topological irregularity causes difficulty in implementing Ampere's law for the time update of the electric field component along the common edge and is responsible for the use of the "nearest neighbor" approximation (CPFDTD).

The topological deficiencies become more problematic, not only for the CPFDTD, but for the CFDTD as well, when the dual grid is inserted. The local nonorthogonal structure of the primary grid and the existence of the "stair steps" result in an unorthodox complex dual grid, which is defined to have its cell vertices located at the barycenters of the primary cells. The basic topological rule that "each dual (primary) grid edge must intersect only one primary (dual) grid face" is violated and therefore algorithmic instability is caused.

Obviously, the two locally conformal FDTD based techniques cannot be extended to the three-dimensional (3-D) modeling of dielectric interfaces unless important alterations in the lattice's structure are performed. It must be mentioned herein that efforts for generalization of the CFDTD method have been recently published [20]–[22]. However, they are based on the introduction of effective permittivities for the edges and cells that intersect the interface (maintaining the Cartesian grid structure in the overall computational domain) and therefore deviate from the original conformal idea.

III. Analysis of the Systematic Procedure

A. Construction of the Locally Conformal Mesh

According to the previous section, the creation of a topologically stable 3-D conformal FDTD algorithm requires the appropriate elimination of the "stair steps." The proposed technique, based on the main idea of the CPFDTD and CFDTD techniques and introducing appropriate grid modifications, overcomes any duality deficiency and constitutes a stable and robust algorithm. A systematic and straightforward way of forming the cells near the dielectric interface can be summarized into the following four-step procedure (pre-processing part of the algorithm).

1) The computational domain is discretized by means of an orthogonal standard FDTD grid.
2) The primary grid cells close to the interface are deformed in order to conform to it and better describe it. The "stair steps," created by cell edges not coinciding with a corresponding edge of a neighboring cell, are detected [Fig. 2(a)].
   a) It is noted that, for curves with less than a 45° slope, the "stair steps" are detected horizontally [i.e., moving along the interface, the cell pair that is responsible for the "stair-step" creation, is detected—the vertical arrow in Fig. 2(a)] and for curves with greater than a 45° slope, the "stair steps" are detected vertically.
   b) In case of curves with a generally varying slope between 0° and 90°, like quarters of circles or ellipses, a combination of the above is used. Simultaneously, the cells containing points with a 45° slope are also detected (transition cell–transition point). Particularly, assuming the upper left quarter of a circle, the search is performed vertically until the transition point of 45° from which further horizontal search is performed as mentioned in Fig. 2(a).
3) In this step, the improved grid is developed by eliminating the "stair steps," and the cells intersected by the interface around the transition point are also reformed.
   a) As far as the "stair steps" concern, the two primary faces that are responsible for their formation are moved toward different directions (opposite to the curve) and the corresponding cells are turned from hexahedrals into five-faced prisms (quadrilaterals into triangles in cross-section view). Therefore, the "stair-step" problem is overcome. This case is illustrated in Fig. 2(b).
   b) For the treatment of the cells around the transition point (45° slope), two cases are distinguished, one in which the transition cell is mostly filled with the material of the cylinder [Fig. 2(c)] and one in which the transition cell is mostly filled with air [Fig. 2(d)], according to the portion of the cell—in which this point is located—that is filled by each dielectric. The diagonal of the cell that intersects almost normally the curve (its two points are located in either side of the curve) is detected. The node of the diagonal, which is closer to the curve, is moved on the diagonal–curve intersection point [1) and 3) of Fig. 2(c) and 1) of Fig. 2(d)]. Furthermore, the edges of the cell that are not connected to the node are completely removed and replaced by the shortened aforementioned diagonal [2) of Fig. 2(c) and (d)]. The two cases are illustrated in Fig. 2(c) and (d).

   The completion of the third step has a consequence: the appearance of five-faced cells at the primary grid, apart from the nonorthogonal hexahedral ones.
4) The dual grid defined by the barycenters of the primary cells' volumes is inserted.

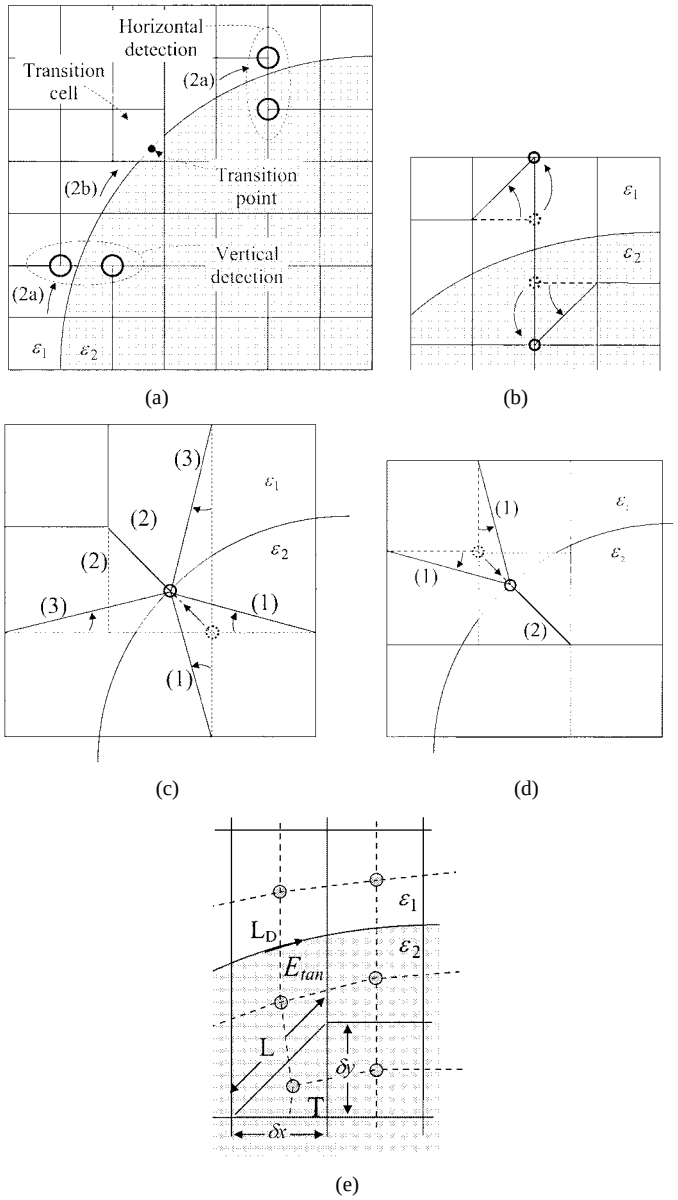

Fig. 2. (a) Cell deformation according to the original CPFDTD and CFDTD methods. The "stair step" (circles) and transition cell detection proceeds as the arrows show. (b) Edge movement and elimination of the "stair steps." (c) Treatment of the transition cells (case 1). (d) Treatment of the transition cells (case 2). (e) Complete modeling according to the systematic procedure (solid lines: primary grid; dashed lines: dual grid; circles: shifted H_z components).

The above four-step procedure can be feasibly implemented for the exact geometric representation of any dielectric interface, needing as a requirement only the knowledge of its variation in space.

B. Update Equations

The update of field components in the grid is performed by means of the integral form of Maxwell's equations, i.e., the circulation of the electric (magnetic) field along the circumference of a primary (dual) grid face is used for the update of the magnetic (electric) field normal to that face. As an example, the algebraic difference equations for the H_z component located at the barycenter of triangle T and of the $E_{\tan}$ component along the interface [Fig. 2(e)], will be derived from Faraday's and Ampere's law, respectively. Therefore, we start from the two integral forms

$$-\iint_{S_T} \frac{\partial \mathbf{B}}{\partial t} \cdot \mathbf{dS} = \oint_{\partial S_T} \mathbf{E} \cdot \mathbf{dl} \tag{1}$$

$$\iint_{S_D} \frac{\partial \mathbf{D}}{\partial t} \cdot \mathbf{dS} = \oint_{\partial S_D} \mathbf{H} \cdot \mathbf{dl} \tag{2}$$

where $\mathbf{E}$ and $\mathbf{H}$ are the electric and magnetic field intensities and $\mathbf{D}$ and $\mathbf{B}$ the electric and magnetic flux densities. Assuming that the flux density normal to a surface and the field intensity along the edge intersecting the surface are related by means of coefficients $P^k_{i,j}$, $k = e, h$, as $\mathbf{D} = \varepsilon \mathbf{E} P^e_{i,j}$ ($\mathbf{B} = \mu \mathbf{H} P^h_{i,j}$), then the algebraic equations derived are the following:

$$\partial_t H_z|^n_{i,j,k} = \frac{-\delta t}{\mu_0 S_T P^h_{i,j}} \left(E_x|^n_{i,j,k} \delta x - E_x|^n_{i,j+1,k} L_T + E_y|^n_{i+1,j,k} \delta y \right) \tag{3}$$

and

$$\partial_t E_{\tan}|^{n+0.5}_{i,j,k} = \frac{\delta t}{\varepsilon L_D \delta z P^e_{i,j}} \left(\begin{array}{l} H_z|^{n+0.5}_{i,j+0.5,k}\, \delta z - H_z|^{n+0.5}_{i,j-0.5,k}\, \delta z - \\ H_y|^{n+0.5}_{i,j,k+0.5}\, L_D + H_y|^{n+0.5}_{i,j,k-0.5}\, L_D \end{array} \right). \tag{4}$$

In (3) and (4), δt is the time step, δz is the edge length along the z-direction, ε and μ are the perimittivity and permeability appointed to the updated component, S_T is the triangle area, L_D is the length of dual edge D, and $L_T = (\delta x^2 + \delta y^2)^{0.5}$. The two important issues of the projection coefficients and the selection of the permittivity of the electric field components along the interface will be defined below.

It must be noted that, if (3) and (4) refer to a standard orthogonal cell, they coincide with the corresponding ones derived by the differential form of Maxwell's equations.

C. Projection Coefficients

The general absence of orthogonality between the primary grid faces/edges and the dual grid edges/faces, due to the local unstructured nature of distorted cells, imposes the use of a projection scheme for the connection of the fluxes computed by Maxwell's equations to the intensities required for this computation [23]. The former are normal to the faces whereas the latter are aligned with the edges. Supposing that an edge intersects its dual face by an angle $\theta^{e,h}$ (Fig. 3), then the following expressions relate a flux (connected to the face) to the corresponding intensity (located along the edge) and define the projection coefficients:

electric field:	$\mathbf{D} = \varepsilon \mathbf{E} \cos\theta^e$	$P^e_{i,j} = \cos\theta^e$
magnetic field:	$\mathbf{B} = \mu_0 \mathbf{H} \cos\theta^h$	$P^h_{i,j} = \cos\theta^h$.

It has to be mentioned that there exist other, more popular projection schemes [6], [24], performing an interpolation of more than one neighboring field intensity components when computing the normal to a face flux density. However, it has been proved that, in general, they lead to late-time instabilities [7], [8]. Although some improvements have been proposed, for simplicity reasons we preferred—and since no inaccuracies are introduced—the above projection scheme.

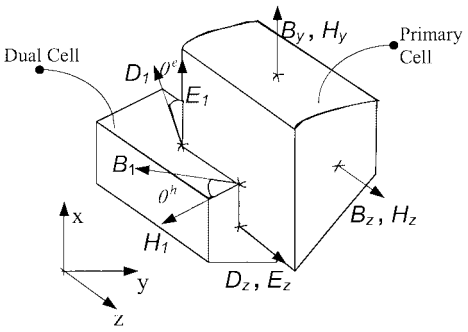

Fig. 3. Field fluxes and intensities are related to each other through a simple geometrical projection.

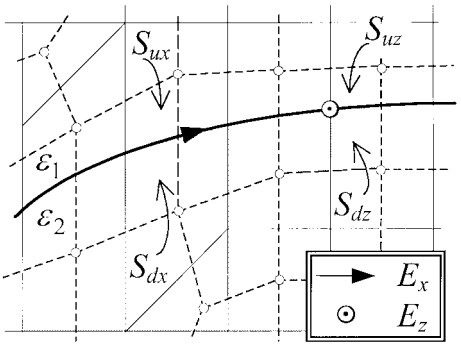

Fig. 4. Computation of the effective perimittivities along the dielectric interface.

D. Effective Permittivities at the Dielectric Interface

When dielectric interfaces are simulated, the permittivity values appointed to the electric field components located along the interface play a very significant role. Considering the interface of Fig. 4, it is only the dielectric constants related to E_x and E_z along the interface that must be appropriately defined. In the proposed method, a scheme based on the discretization of the integral form of Maxwell's equations over finite volumes containing the interface, and taking into account the continuity

conditions across it, is implemented. Therefore, the following effective permittivities are derived:

$$\varepsilon_{rx}^{\text{eff}} = \frac{S_{ux}\delta z\varepsilon_1 + S_{dx}\delta z\varepsilon_2}{S_{ux}\delta z + S_{dx}\delta z} = \frac{S_{ux}\varepsilon_1 + S_{dx}\varepsilon_2}{S_{ux} + S_{dx}}$$

$$\varepsilon_{rz}^{\text{eff}} = \frac{S_{uz}\delta z\varepsilon_1 + S_{dz}\delta z\varepsilon_2}{S_{uz}\delta z + S_{dz}\delta z} = \frac{S_{uz}\varepsilon_1 + S_{dz}\varepsilon_2}{S_{uz} + S_{dz}}$$

where S_u and S_d are the areas of the cell belonging to the material with permittivities ε_1 and ε_2, respectively. These values, which are the outcome of linear weighting in the volume of a cell, are proved to maintain the second order accuracy of the FDTD equations [25].

E. Stability Analysis

As has already been mentioned, the numerical stability of the proposed scheme must be examined from two points of view: the topological one and the time discretization one.

To probe further, we assume that the update equations can be written in a matrix form by means of the following coupled set of first-order difference equations:

$$\mathbf{b}^{n+0.5} = \mathbf{b}^{n-0.5} - \delta t C_e D_\varepsilon A_d \mathbf{d}^n \tag{5}$$

$$\mathbf{d}^{n+1} = \mathbf{d}^n + \delta t C_h A_b \mathbf{b}^{n+0.5} \tag{6}$$

where $\mathbf{d}$, $\mathbf{b}$ are vectors of the discrete flux density components, the superscripts refer to discrete time, C_e and C_h represent the discrete contour integrals of the electric and magnetic fields around primary and secondary cell faces, respectively, D_ε is a diagonal matrix having as elements the inverse of the relative permittivity, and A_b and A_d are the projection matrices. According to the analysis of [7], the system eigenvalue equation and the system matrix can be derived, leading to the following two conditions that need to be satisfied in order to assure stability:

1) The system matrix must be positive definite with real and distinct eigenvalues (topology).
2) The time step (time discretization) must be less than $2/(\sup\{\sqrt{C_h A_b C_e D_\varepsilon A_d}\})$.

In the proposed scheme, matrices A_b and A_d are diagonal (each flux component is connected only to one intensity component as mentioned in Section III-C) and, therefore, symmetric and positive definite. Moreover, matrix D_ε is also diagonal even for inhomogeneous domains. Therefore, and since the product $C_h C_e$ is always positive definite, the former condition is satisfied and the algorithm does not suffer from late-time instabilities, which are the outcome of a nonsymmetric or nonpositive definite system matrix. On the other hand, the second condition is equivalent to the one derived in [26] as a function of the metric coefficients of a general curvilinear space. However, the maximum value of the time step that does not lead to instability may also be defined by the empirical, though fairly practical, relation (similar to the one of the PGY algorithm [24])

$$\delta t \le \left[c_d \max\left\{ \sqrt{\left(\frac{1}{\delta z}\right)^2 + \left(\frac{1}{l_{k1}}\right)^2 + \left(\frac{1}{l_{k2}}\right)^2} \right\} \right]^{-1}$$

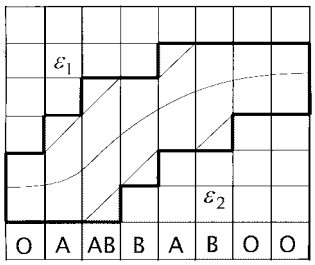

Fig. 5. Four distinct regions of the primary grid as they are formed for the simulation of an arbitrary curve. The dual grid is correspondingly created.

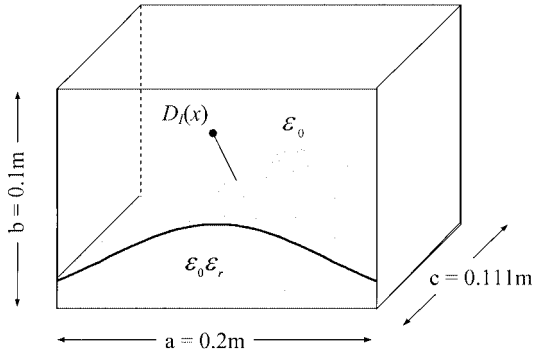

Fig. 6. Partially filled resonator.

where c_d is the speed of light in the material with minimum permittivity and l_{k1} and l_{k2} are the length of edges sharing a common vertice.

Therefore, the avoidance of any approximation schemes (such as "nearest-neighbor"), together with the implementation in the procedure of simple projection coefficients and effective relative permittivities, assures algorithmic accuracy and stability.

F. Discussion

Apparently, the proposed technique preserves, in a major level, the characteristics of the original FDTD method, since the deformed cells exist only in a three-cell width area across the simulated surface (interface). Therefore, the additional memory requirements of the algorithm, since they are related only to the edge lengths and areas of the distorted cells as well as to the projection coefficients for each edge-face pair, are insignificant. Furthermore, the overall computational time is slightly larger than the one required by the standard FDTD method, with staircase meshing or special effective coefficient schemes, with the same grid size. These extra demands correspond to the preprocessing part of the procedure, where all the geometric information is calculated and stored. On the other hand, the iteration part requires no more computational time than that of the standard FDTD algorithm. Nevertheless, the accuracy obtained by the innovative technique is much higher, as will be revealed by the numerical results.

Moreover, the mesh generation performed in the preprocessing part may be realized in a feasible and systematic way. This can be attained via several procedures. We indicate below the idea on which we were based, a characterization of various types of cell areas around the curved interface that require special treatment. Specifically, four types of cell areas in the

TABLE I
RESONANT FREQUENCIES ($\times 10^8$) FOR $\varepsilon_r = 38$ ($A \equiv$ PROPOSED METHOD, $B \equiv$ STAIRCASE FDTD METHOD, $C \equiv$ METHOD [22])

No of cross-section cells	$q = 1$			$q = 2$			$q = 3$		
	A	**B**	**C**	**A**	**B**	**C**	**A**	**B**	**C**
30	5.0754	4.7751	4.7425	5.2035	5.0195	4.9380	6.2015	5.8835	5.851
110	5.0395	5.043	5.075	5.3010	5.1380	5.0908	6.2250	6.0868	6.1026
440	5.059	5.059	5.091	5.3196	5.1225	5.1230	6.1884	6.1342	6.1342
990	5.075	5.075	5.085	5.3121	5.3121	5.3121	6.1660	6.1184	6.1469
1760	5.06	5.0592	5.06	5.2973	5.3121	5.3121	6.1435	6.134	6.134

TABLE II
RESONANT FREQUENCIES ($\times 10^8$) FOR $Q = 2$ ($A \equiv$ PROPOSED METHOD, $B \equiv$ STAIRCASE FDTD METHOD, $C \equiv$ METHOD [22])

No of cross-section cells	$\varepsilon_r = 2.495$			$\varepsilon_r = 20$			$\varepsilon_r = 38$		
	A	**B**	**C**	**A**	**B**	**C**	**A**	**B**	**C**
30	17.263	16.363	16.036	6.9147	6.7145	6.4211	5.0521	4.9055	4.6936
110	17.281	16.474	16.490	6.9344	6.8457	6.7824	5.0755	5.0118	4.9643
440	16.926	16.442	16.493	6.8819	6.7983	6.7983	5.0220	4.9643	4.9643
990	16.785	16.468	16.506	6.8819	6.7919	6.8299	4.9996	4.9801	5.0086
1760	16.703	16.474	16.506	6.8448	6.8299	6.7983	4.9996	4.9959	4.9643

primary grid can be distinguished according to the slope angle of the dielectric interface:

- region "A": column containing one (1) five-faced prismatic cell (prism of triangular cross-section) above the dielectric interface;
- region "B": column containing one (1) five-faced prismatic cell below the dielectric interface;
- region "AB": column containing two (2) five-faced prismatic cells, one above and one below the dielectric interface;
- region "O": column containing no five-faced prismatic cells.

It must be mentioned that a single "stair step" is replaced via the above procedure by a pair of regions "A" and "B." However, when the curve is very steep, $k > 1$ subsequent "stair steps" appear in the grid, which are substituted by one region "A," $k-1$ regions "AB," and one region "B." Regions "O" describe the classical, distorted, hexahedral cells in the absence of "stair steps." Fig. 5 depicts in the cross-sectional view the discretization of the interface between two dielectrics by the proposed method. This distinction, while requiring minor computer resources, greatly simplifies the algorithm.

Finally, in the case of interfaces with a generally varying slope, the transition cells are easily detected and reformed according to the procedure given in Section III-A.

IV. NUMERICAL RESULTS

The proposed methodology is validated through the analysis of various resonant structures, constituting challenging numerical problems since late-time instabilities are often reported due to the absence of dissipation for spuriously generated energy. Additionally, the greater sensitivity of the results to any lattice inaccuracies, as compared to scattering problems, renders the selected ones even more appropriate for the validation of our scheme. The resonant frequencies are computed for each case and compared either with analytical/experimental values or with results obtained by the utilization of other methods.

It is also mentioned that all frequency-domain results are extracted from the implementation of the Fourier transform on the time samples filtered by a Blackman–Harris window.

A. Partially Filled Orthogonal Cavities

The resonant cavity (Fig. 6) has the dimensions $0.2 \times 0.1 \times 0.111$ m^3 is excited by a Gaussian in space and time distribution and is characterized by a dielectric interface that varies according to the function [27]

$$D_I(x) = \frac{b}{2}\left(0.01 + 0.99\exp\left(-q^2\left(x/a - 0.5\right)^2\right)\right)$$

where a and b are the width and the height of the structure and q a curvature parameter.

The results derived by the innovative lattice structure are compared with those of the staircase FDTD technique and of a variation of the CFDTD technique [22].

Specifically, the efficiency of the proposed algorithm is tested for a series of different interface curvatures obtained by varying parameter q, while the filling material remains the same ($\varepsilon_r = 38$). The results are shown in Table I where the fourth resonant frequency of the cavity for three values of q ($q = 1, 2, 3$) is computed. The promising performance of the new scheme is obvious, since even for very coarse meshes it is significantly accurate. Furthermore, no instabilities are observed as the grid

TABLE III
COMPARISON OF THE COMPUTATIONAL RESOURCES CALCULATION OF THE FOURTH RESONANT FREQUENCY FOR $Q = 3$ AND $\varepsilon_r = 38$

No of cross-section cells	Proposed Method			Staircase/[22] Methods		
	CPU time	Memory (MB)	Frequency ($\times 10^8$)	CPU time	Memory (MB)	Frequency ($\times 10^8$)
30	14"	0.066	6.2015	8"	0.046	5.851
110	2' 10"	0.174	6.2156	1' 52"	0.150	6.1026
440	21' 58"	1.30	6.1884	17' 22"	1.07	6.1342
990	1h 25'	4.34	6.166	1h 21'	3.37	6.1184
1760	6h 57'	10.24	6.1435	6h 53'	7.67	6.134

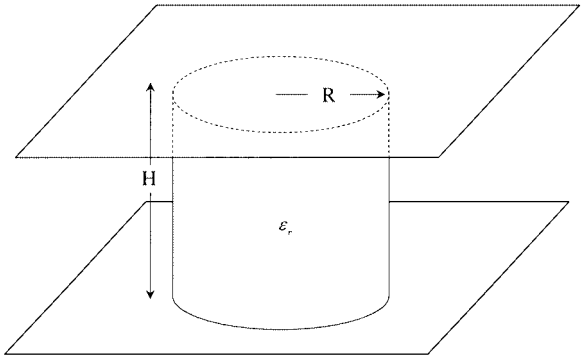

Fig. 7. Parallel-plate dielectric resonator with $R = 5.25$ mm, $H = 4.62$ mm, and relative dielectric constant $\varepsilon_r = 38$.

TABLE IV
HIGHER ORDER RESONANT FREQUENCIES (IN GIGAHERTZ) OF THE PARALLEL-PLATE DIELECTRIC RESONATOR

Modes	Analytical values	Proposed Conf. FDTD		Axially sym. FDTD [4]	
		Frequency	Rel. error(%)	Frequency	Rel. error(%)
HEM_{211}	7.4995	7.4961	+ 0.0453	7.4979	0.0213
HEM_{121}	8.3177	8.3275	- 0.1178	8.3172	0.0060
HEM_{311}	9.0250	9.0320	- 0.0775	8.9922	0.3634
HEM_{221}	9.7139	9.7400	- 0.2679	9.6995	0.1482
HEM_{212}	11.8310	11.8025	+ 0.2408	11.8217	0.0786
HEM_{312}	12.8107	12.8000	+ 0.0835	12.7618	0.3817
HEM_{331}	13.3215	13.3740	- 0.3940	13.2316	0.6478

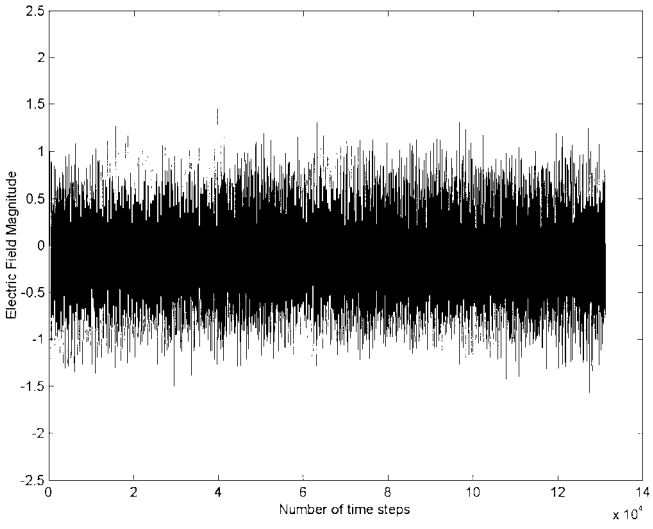

Fig. 8. Electric field intensity variations versus time.

becomes denser despite the large number of time steps that were used so as to examine the limits of the algorithm.

The proposed technique was also tested for various values of the filling material permittivity, since a higher dielectric discontinuity is more difficult to be accurately modeled. Nevertheless, as shown in Table II, the new scheme preserves its accuracy thanks to the precise geometric representation of the interface and the use of the effective permittivity scheme along the interface.

Consequently, the overall computational resources needed for a specific level of accuracy is significantly reduced as proved by the comparative study of Table III, where the CPU time and memory requirements of the three methods and the fourth resonant frequency computed by them for various grids, are listed. This important advantage of the proposed methodology is based on its ability to obtain significant precision while simultaneously maintaining in a major level the simple and easy-to-program structure of the standard FDTD algorithm.

It is worth mentioning that the resonant frequencies computed by the proposed technique approaches the exact value from above. This property, observed in most of the cases treated, is appointed to the utilization of the projection coefficients, which affect the dispersion relation.

B. Parallel-Plate Cylindrical Dielectric Resonator

The resonant frequencies of the parallel-plate dielectric resonator of Fig. 7 are computed by means of the proposed algorithm. For this simulation, δx and δy were set equal to 0.25 R, the number of time steps was 32 768, whereas the computational domain along the x- and y-directions was truncated by a six-layer perfectly matched layer (PML). In contrast to the previous problem, the curvature range of the interface is greater and requires, for proper modeling, the utilization of transition cells as well. Nevertheless, and despite the coarse mesh used, the accuracy obtained is very good (the relative error is quite small even for the higher order modes) as revealed by the comparison of the

TABLE V
HIGHER ORDER RESONANT FREQUENCIES (IN GIGAHERTZ) OF THE CYLINDRICAL DIELECTRIC RESONATOR

Modes	Experimental values [5]	Proposed	Axially sym. FDTD [5]
TE_{H01}	4.85	4.855	4.848
HE_{H11}	–	6.315	6.310
HE_{E11}	6.64	6.667	6.638
TM_{E01}	7.60	7.586	7.513
HE_{E21}	7.81	7.860	7.721
TE_{E01}	–	8.330	8.297
HE_{H21}	–	8.490	8.455
TE_{H02}	–	9.120	9.100
HE_{H12}	–	9.338	9.350
HE_{H13}	–	9.925	9.920

results with analytical values and those of a dense 2-D FDTD (body of revolution) method [4], presented in Table IV. Moreover, the stability of the algorithm is demonstrated in Fig. 8, where time samples of the electric field inside the resonator are shown (in this case the number of time steps was 131 072).

C. Cylindrical Dielectric Resonator

The cylindrical dielectric resonator (without parallel plates) constitutes an open problem requiring additional mesh truncation (PML) along the z-direction. This did not cause a stability problem since, similarly to the proposed algorithm, the PML is also planar. The dimensions and the permittivity as well as the characteristics of the grid used are equal to those of the previous problem. Again, a very close agreement between the resonant frequencies computed, the experimental values, and the ones of a dense 2-D FDTD (body of revolution) method [5] (see Table V) is observed and proves the validity of the algorithm.

V. CONCLUSION

A systematic and feasible procedure for the direct conformal simulation of nonorthogonal dielectric structures in three dimensions was introduced. It is based on a successful combination of prism and hexahedral cells which restore the duality of the two grids that is violated by the traditional CPFDTD and CFDTD techniques when implemented in dielectric interfaces. Therefore, a topologically stable numerical tool was produced that proved to be fairly efficient in the analysis of partially filled and dielectric resonators.

REFERENCES

[1] A. Taflove, *Computational Electrodynamics. The Finite-Difference Time-Domain Method*. Norwood, MA: Artech House, 1995.
[2] R. Holland, "Pitfalls of staircase meshing," *IEEE Trans. Electromagn. Compat.*, vol. 35, pp. 434–439, Nov. 1993.
[3] A. C. Cangellaris and D. B. Wright, "Analysis of the numerical error caused by the stair-stepped approximation of a conducting boundary in FDTD simulations of electromagnetic phenomena," *IEEE Trans. Antennas Propagat.*, vol. 39, pp. 1518–1525, Oct. 1991.
[4] S. Shi, L. Yang, and D. W. Prather, "Numerical study of axisymmetric dielectric resonators," *IEEE Trans. Microwave Theory Tech.*, vol. 49, pp. 1614–1619, Sept. 2001.
[5] A. Navarro and M. J. Nunez, "FDTD method coupled with FFT: A generalization to open cylindrical devices," *IEEE Trans. Microwave Theory Tech.*, vol. 42, pp. 870–874, May 1994.
[6] N. K. Madsen, "Divergence preserving discrete surface integral methods for Maxwell's curl equations using nonorthogonal unstructured grids," *J. Comput. Phys.*, vol. 119, pp. 34–45, 1995.
[7] S. D. Gedney and J. A. Roden, "Numerical stability of nonorthogonal FDTD methods," *IEEE Trans. Antennas Propagat.*, vol. 48, pp. 231–239, Feb. 2000.
[8] R. Schuhmann and T. Weiland, "Stability of the FDTD algorithm on nonorthogonal grids related to the spatial interpolation scheme," *IEEE Trans. Magn.*, vol. 34, pp. 2751–2754, Sept. 1998.
[9] ——, "FDTD on nonorthogonal grids with triangular fillings," *IEEE Trans. Magn.*, vol. 35, pp. 1470–1473, May 1999.
[10] T. Jurgens, A. Taflove, K. Umashankar, and T. G. Moore, "Finite-difference time-domain modeling of curved surfaces," *IEEE Trans. Antennas Propagat.*, vol. 40, pp. 357–365, Apr. 1992.
[11] T. G. Jurgens and A. Taflove, "Three-dimensional contour FDTD modeling of scattering from single and multiple bodies," *IEEE Trans. Antennas Propagat.*, vol. 41, pp. 1703–1708, Dec. 1993.
[12] S. Dey and R. Mittra, "A locally conformal finite-difference time-domain (FDTD) algorithm for modeling three-dimensional perfectly conducting objects," *IEEE Microwave Guided Wave Lett.*, vol. 7, pp. 273–275, Sept. 1997.
[13] C. J. Railton, "An algorithm for the treatment of curved metallic laminas in the finite difference time domain method," *IEEE Trans. Microwave Theory Tech.*, vol. 41, pp. 1429–1438, Aug. 1993.
[14] J. Fang and J. Ren, "A locally conformed finite-difference time-domain algorithm of modeling arbitrary shape planar metal strips," *IEEE Trans. Microwave Theory Tech.*, vol. 41, pp. 830–838, May 1993.
[15] C. J. Railton and I. J. Craddock, "Stabilized CPFDTD algorithm for the analysis of arbitrary 3D, PEC structures," *Proc. Inst.Elect. Eng.*, pt. H, vol. 143, pp. 367–372, Oct. 1996.
[16] C. Railton and J. Schneider, "An analytical and numerical analysis of several locally conformal FDTD schemes," *IEEE Trans. Microwave Theory Tech.*, vol. 47, pp. 56–66, Jan. 1999.
[17] W. Yu and R. Mittra, "A conformal FDTD algorithm for modeling perfectly conducting objects with curve-shaped surfaces and edges," *Microwave Opt. Technol. Lett.*, vol. 27, pp. 136–138, 2000.
[18] I. J. Craddock, C. J. Railton, and J. P. McGeehan, "Derivation and application of passive equivalent circuit for the finite difference time domain algorithm," *IEEE Microwave Guided Wave Lett.*, vol. 6, pp. 40–42, Jan. 1996.
[19] Y. Hao and C. J. Railton, "Analyzing electromagnetic structures with curved boundaries on Cartesian FDTD meshes," *IEEE Trans. Microwave Theory Tech.*, vol. 46, pp. 82–88, Jan. 1998.
[20] S. Dey and R. Mittra, "A conformal finite-difference time-domain technique for modeling cylindrical dielectric resonators," *IEEE Trans. Microwave Theory Tech.*, vol. 47, pp. 1737–1739, Sept. 1999.
[21] N. Kaneda, B. Houshmand, and T. Itoh, "FDTD analysis of dielectric resonators with curved surfaces," *IEEE Trans. Microwave Theory Tech.*, vol. 45, pp. 1645–1649, Sept. 1997.
[22] W. Yu and R. Mittra, "A conformal finite difference time domain technique for modeling curved dielectric surfaces," *IEEE Microwave Wireless Comp. Lett.*, vol. 11, pp. 25–27, Jan. 2001.
[23] T. I. Kosmanis and T. D. Tsiboukis, "A systematic conformal finite-difference time-domain (FDTD) technique for the simulation of arbitrarily curved interfaces between dielectrics," *IEEE Trans. Magn.*, vol. 38, pp. 645–648, Mar. 2002.
[24] S. D. Gedney, F. S. Lansing, and D. L. Rascoe, "Full wave analysis of microwave monolithic circuit devices using a generalized Yee-algorithm based on an unstructured grid," *IEEE Trans. Microwave Theory Tech.*, vol. 44, pp. 1393–1400, Aug. 1996.
[25] K.-P. Hwang and A. C. Cangellaris, "Effective permittivities for second-order accurate FDTD equations at dielectric interfaces," *IEEE Microwave Wireless Comp. Lett.*, vol. 11, pp. 158–160, Apr. 2001.

[26] J.-F. Lee, R. Palandech, and R. Mittra, "Modeling three-dimensional discontinuities in waveguides using nonorthogonal FDTD algorithm," *IEEE Trans. Microwave Theory Tech.*, vol. 40, pp. 346–352, Feb. 1992.
[27] A. Ioffe and A. Dreher, "Discrete mode matching method for the analysis of quasiplanar structures," in *Dig. IEEE AP-S Int. Symp.–URSI Radio Sci. Meet.*, Orlando, FL, July 1999, pp. 1840–1843.

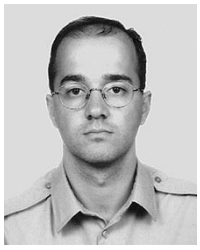

Theodoros I. Kosmanis (S'96) was born in Thessaloniki, Greece, in 1974. He received the Diploma degree (with honors) in electrical and computer engineering and Ph.D. degree from the Aristotle University of Thessaloniki, Thessaloniki, Greece, in 1997 and in 2002, respectively.

From 1997 to 2002, he was a Research and Teaching Assistant with the Department of Electrical and Computer Engineering, Aristotle University of Thessaloniki. His current research interests include computational electromagnetics and especially classical and CFDTD techniques and the finite-element method (FEM). He is also interested in spectrum estimation techniques (Prony, wavelets, AR- and ARMA models).

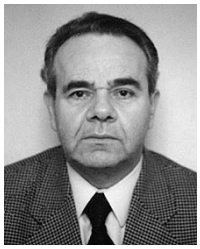

Theodoros D. Tsiboukis (S'79–M'81–SM'99) received the Diploma degree in electrical and mechanical engineering from the National Technical University of Athens, Athens, Greece, in 1971, and the Doctor Engineer Degree from the Aristotle University of Thessaloniki (AUTH), Thessaloniki, Greece, in 1981.

From 1981 to 1982, he was with the Electrical Engineering Department, University of Southampton, Southampton, U.K., as a Senior Research Fellow. Since 1982, he has been with the Department of Electrical and Computer Engineering (DECE), AUTH, where he is currently a Professor. He has served in many administrative positions, including Director of the Division of Telecommunications at the DECE (1993–1998) and Chairman of the DECE (1997–1998). His main research interests include electromagnetic field analysis by energy methods, computational electromagnetics [FEM, boundary-element method (BEM), vector finite elements, method of moments (MoM), FDTD, absorbing boundary conditions (ABCs)], and inverse and electromagnetic compatibility (EMC) problems. He has authored or coauthored six books, over 85 refereed journal papers, and over 80 international conference papers. He was the Guest Editor of a Special Issue of the *International Journal of Theoretical Electrotechnics* (1996).

Dr. Tsiboukis is member of various societies, associations, chambers, and institutions. He was the chairman of the local organizing committee of the 8th International Symposium on Theoretical Electrical Engineering (1995). He has been the recipient of several distinctions.